Significance of Miscibility in Multidonor Bulk Heterojunction Solar Cells

Benjamin F. Hartmeier,[1,2] Michael A. Brady,[1] Neil D. Treat,[1] Maxwell J. Robb,[3] Thomas E. Mates,[4] Alexander Hexemer,[5] Cheng Wang,[5] Craig J. Hawker,[1,3,4] Edward J. Kramer,[1,6†] Michael L. Chabinyc[1]

[1]Materials Department, University of California, Santa Barbara, California 93106
[2]Department of Materials, ETH Zürich, Vladimir-Prelog-Weg 5, Zürich CH-8093, Switzerland
[3]Department of Chemistry and Biochemistry, University of California, Santa Barbara, California 93106
[4]Materials Research Laboratory, University of California, Santa Barbara, California 93106
[5]Lawrence Berkeley National Laboratory, Advanced Light Source, Berkeley, California 94720
[6]Department of Chemical Engineering, University of California, Santa Barbara, California 93106
Correspondence to: M. L. Chabinyc (E-mail: mchabinyc@engineering.ucsb.edu)

Received 14 July 2015; accepted 31 August 2015; published online 00 Month 2015
DOI: 10.1002/polb.23907

ABSTRACT: Ternary organic blends have potential in realizing efficient bulk heterojunction (BHJ) organic solar cells by harvesting a larger portion of the solar spectrum than binary blends. Several challenging requirements, based on the electronic structure of the components of the ternary blend and their nanoscale morphology, need to be met in order to achieve high power conversion efficiency in ternary BHJs. The properties of a model ternary system comprising two donor polymers, poly(3-hexylthiophene) (P3HT) and a furan-containing, diketopyrrolopyrrole-thiophene low-bandgap polymer (PDPP2FT), with a fullerene acceptor, $PC_{61}BM$, were examined. The relative miscibility of $PC_{61}BM$ with P3HT and PDPP2FT was examined using diffusion with dynamic secondary ion mass spectrometry (dynamic SIMS) measurements. Grazing incidence small and wide angle X-ray scattering analysis (GISAXS and GIWAXS) were used to study the morphology of the ternary blends. These measurements, along with optoelectronic characterization of ternary blend solar cells, indicate that the miscibility of the fullerene acceptor and donor polymers is a critical factor in the performance in a ternary cell. A guideline that the miscibility of the fullerene in the two polymers should be matched is proposed and further substantiated by examination of known well-performing ternary blends. The ternary blending of semiconducting components can improve the power conversion efficiency of bulk heterojunction organic photovoltaics. The blending of P3HT and PDPP2FT with $PC_{61}BM$ leads to good absorptive coverage of the incident solar spectrum and cascading transport energy levels. The performance of this ternary blend reveals the impact of the miscibility of $PC_{61}BM$ in each polymer as a function of composition, highlighting an important factor for optimization of ternary BHJs. © 2015 Wiley Periodicals, Inc. J. Polym. Sci., Part B: Polym. Phys. **2015**, *00*, 000–000

KEYWORDS: donor-donor-acceptor blend; organic photovoltaics; polymer-fullerene miscibility; semiconducting polymer; ternary bulk heterojunction

INTRODUCTION Semiconducting polymers have been the focus of intense investigation because of their potential application in inexpensive, flexible electronics, including organic light emitting diodes (OLEDs),[1] thin film transistors (OTFTs),[2] photovoltaic solar cells (OPVs),[3] and thermoelectrics.[4] These materials are processable using solution deposition techniques, providing flexibility in methods to fabricate devices. Consequently, OPVs have been considered as an alternative to conventional inorganic thin film solar cells.[5–7] The power conversion efficiency (PCE) of OPVs is currently near 10%, but there is a need to significantly enhance this efficiency.[8,9]

The highest-performance OPVs are currently based on the bulk heterojunction (BHJ) strategy, where electron-donating and electron-accepting materials are blended together into a bicontinuous network with nanoscale phase separation.[5,10] A critical limitation in the PCE of BHJ OPVs is the relatively narrow width of the optical absorption of organic materials and

†Deceased December 2014.

Additional Supporting Information may be found in the online version of this article.

© 2015 Wiley Periodicals, Inc.

their alignment with the incident solar spectrum.[10,11] For example, in the well-studied model system, poly(3-hexylthiophene):[6,6]-phenyl-C_{61}-butyric acid methyl ester (P3HT:$PC_{61}BM$), the donor polymer P3HT absorbs primarily in the range of 400 to 650 nm, which misses a large portion of the solar spectrum.[12]

An effective strategy to enhance the PCE of OPVs is to improve the overlap of the optical absorption of the BHJ layer with the solar spectrum. This goal has been addressed by tuning the electronic structure of the donor polymer to lower the optical gap,[13–17] or alternatively through the addition of another material to form a ternary BHJ.[18–26] The additional material is chosen in a complementary way with the other materials in the binary blend to improve the overlap with the solar spectrum. In the design of this complementary absorber, the offsets of the electronic levels and the ability to extract free charge carriers must be considered. For example in one strategy to design a complementary donor for a P3HT:$PC_{61}BM$ BHJ, the ionization energy (IE) of the complementary absorber should be smaller than that for $PC_{61}BM$ and larger than that for P3HT in order for hole collection to occur. In addition, the electron affinity (EA) should be smaller than that of $PC_{61}BM$ and larger than that of P3HT in order to facilitate efficient electron collection by the fullerene. Such an arrangement of cascading energy levels is likely to prevent charge trapping, assuming the carriers can freely access each component of the ternary blend.

There have been many reports of forming ternary solar cells by blending two donor polymers and one fullerene-based electron acceptor.[18–23,25–41] Overall, these findings suggest that addition of a complementary absorber can improve the short-circuit current (J_{SC}), and thereby the PCE, by 25 to 30% in some cases. An interesting observation in many of these ternary cells is the change in open circuit voltage (V_{oc}) with composition, suggesting that the donor polymers behave as an electronic alloy.[18,30–33,40,41] The origin of this behavior appears to be dependent on the ability of the polymers to mix, but the effect is still not fully understood.

We present here a study of ternary BHJs using P3HT and the furan-containing, diketopyrrolopyrrole-thiophene low-bandgap polymer PDPP2FT[14,17] with $PC_{61}BM$. As depicted schematically in Figure 1, we discuss a critical design consideration for ternary blend OPVs:[42] the relative interaction of $PC_{61}BM$ with each donor polymer. This compositional study of ternary solar cells comprising P3HT and PDPP2FT provides a morphological origin for the electronic behavior of these BHJs. Interdiffusion[43,44] and X-ray scattering experiments were carried out to help understand the significant changes in performance observed in solar cells as the ternary blend composition is varied. The miscibility of the fullerene with the donor polymers was found to be a critical parameter controlling the performance of ternary BHJs.

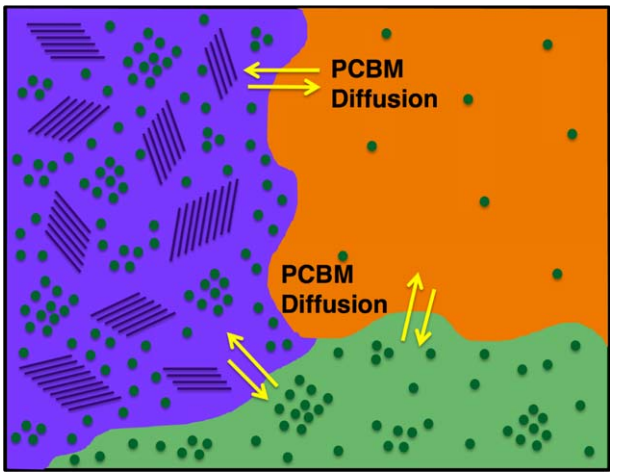

FIGURE 1 Schematic representation of the domain structure and interdiffusion-driven miscibility differences in the P3HT:PDPP2FT:$PC_{61}BM$ ternary blend. P3HT, PDFF2FT, and $PC_{61}BM$ regions are displayed in purple, orange, and green, respectively. P3HT crystallites and both aggregated and molecularly dispersed $PC_{61}BM$ are shown in detail.

EXPERIMENTAL

Materials used in this work include P3HT Sepiolid P200 (BASF), (penta-deuterated) $PC_{61}BM$ (Nano-C and Sigma-Aldrich), and silicon- and carbon-bridged PCPDTBT (Konarka and 1-Material). PDPP2FT was prepared according to literature reports.[14,45] All materials were used as received and were stored and processed in a nitrogen atmosphere. All active layer materials were dissolved in chlorobenzene at concentrations of 10 to 45 mg/mL, respecting the maximum solubility and final solution viscosity.

Solar cells were produced on 1.5 × 1.5 cm^2 sized glass slides, precoated with indium doped tin oxide (ITO) by TFD Co. The slides were cleaned in a four-step process, involving ultrasonication for 10 min each in acetone, 2 vol % alconox® solution, distilled water, and isopropyl alcohol. Aqueous PEDOT:PSS solution (Clevios P VP AI 4083) was subsequently spin coated onto the plasma cleaned ITO slides, and deposited films were annealed at 140 °C to remove residual water. The active layer solutions were mixed from stock solutions, and their relative concentrations were varied. Ratios for the polymer:$PC_{61}BM$ ratio for BHJs were taken from existing reports and followed even in ternary blends, thus changing the absolute amount of $PC_{61}BM$ for changing ratios of polymers (see Supporting Information). Subsequently the active layers were spin coated at 1000 to 2000 rpm, depending on the expected viscosity of the solution. The layers were then annealed, and a 10 nm/100 nm calcium/aluminum back contact was evaporated under high vacuum. *J–V* and EQE curves were then measured with a previously calibrated solar simulator and monochromator, respectively.

In the compositional space studied here, both the P3HT:PDPP2FT and $PC_{61}BM$:total polymer composition ratios are changing. The relative weight ratio of $PC_{61}BM$ to total donor polymer is changed as the fraction of PDPP2FT is modulated. This change in fullerene fraction as the polymer

A/polymer B ratio is adjusted was utilized in order to achieve the necessary polymer:fullerene ratio in the blend. The two polymer-fullerene binary blends have significantly different endpoints; therefore, the total polymer-fullerene blend ratio is linearly varying between that of P3HT:$PC_{61}BM$ (1:1) and that of PDPP2FT:$PC_{61}BM$ (1:3), as the PDPP2FT fraction is increased (and the P3HT fraction correspondingly decreased).

The bilayer diffusion measurements were conducted in a similar manner as previously reported.[43,44] All layers were separately cast onto pieces of single crystal silicon wafer, covered with a thermal oxide of 150 nm thickness and cleaned in the same way as ITO slides, explained above. All other solutions, pure donor polymer and donor-acceptor blends, were mixed from stock solutions to concentrations between 10 mg/mL and 30 mg/mL and spin coated at 1000 to 2000 rpm, depending on the desired layer thickness. The two corresponding layers were laminated by dipping the pure polymer layer into a 5 vol % solution of hydrofluoric acid, floating the detached layer onto a water surface, and picking it up by the substrate layer containing the pure or mixed $dPC_{61}BM$. This process was used to inhibit premature diffusion by solvents or heat, used in other lamination techniques. The bilayer was then annealed to activate the desired diffusion at various temperatures for 5 min on a hot plate within a N_2 atmosphere glove box. Finally, a sacrificial layer of polystyrene was spin coated from toluene solution and laminated on top of the annealed bilayer in the same way as described for bilayer lamination by film floating. The composition as a function of depth was measured with a Physical Electronics 6650 Quadrupole SIMS instrument. Oxygen O_2^- primary ions were generated at 2 kV and 45 nA and rastered over a square of area (300 μm)^2 on the sample surface. An electron gun was aimed onto the same spot to counterbalance the charging of the sample. Hydrogen ^{1}H, deuterium ^{2}H, carbon ^{12}C, silicon ^{28}Si, sulfur ^{34}S, ^{26}CN, and ^{27}HCN negative ions were monitored. The PS sacrificial layer was used to reduce measurement artifacts from electron gun interaction with the sample and also intensity variations at the beginning of the SIMS measurement. A PS/d-PS/PS trilayer sample, of known deuteration chemistry, was analyzed in order to calibrate the $^2H^-/^1H^-$ signal ratio.

The X-ray scattering measurements (GIWAXS & GISAXS) were conducted at Beamline 7.3.3 at the Advanced Light Source (ALS) at Lawrence Berkeley National Laboratory (LBNL). Pure polymer layers and binary and ternary blends were spin coated onto pieces of silicon wafers with native oxide layers, and some were annealed at 110 °C for 5 min to simulate solar cell conditions. The acquired images were normalized with a AgB standard; vertical $\boldsymbol{q_z}$ and horizontal $\boldsymbol{q_{xy}}$ line cuts (GIWAXS) and horizontal $\boldsymbol{q_y}$ line cuts (GISAXS) were used for qualitative data evaluation.

RESULTS AND DISCUSSION

A key goal of the development of ternary blend OPVs is broad spectral absorption. With P3HT:$PC_{61}BM$ as the model binary blend, PDPP2FT was chosen as the complementary, low bandgap donor polymer [Fig. 2(a)]. These two polymers have cascading electronic levels, as seen in Figure 2(b), enabling exciton dissociation at interfaces of both P3HT and PDPP2FT with $PC_{61}BM$ and also at interfaces of P3HT and PDPP2FT. Charge transport should be preferred in PCBM and P3HT due to their EA and IE, assuming the carriers reach these sites before extraction or recombination. Their absorption spectra are complementary and provide substantial coverage of the solar spectrum, with PDPP2FT having an absorption peak higher in energy than that of P3HT, and also one in the near-IR range [Fig. 2(c)]. Thus, if the microstructure can be optimized for charge generation and transport, these two donor polymers are a good complementary pair for application in ternary blends.

Relative Miscibility of $PC_{61}BM$ in P3HT and PDPP2FT

The miscibility of fullerenes in polymers has been suggested to be an important factor in determining the efficiency of charge generation and the overall PCE of BHJs.[43,44,46] The impact of miscibility on morphology in thin films of ternary BHJs is particularly difficult to study due to the complex nanostructure that comprises three semicrystalline and aggregated components, in addition to amorphous, mixed-composition domains.[46] Previously, we have found dynamic secondary ion mass spectrometry (dynamic SIMS) to be a helpful technique for determining the solid-state miscibility of $PC_{61}BM$ in P3HT in thin films.[43] Here, we use a modification of this method to examine how composition is affected by the presence of a secondary polymer in ternary blends by studying model diffusion couples.

Temperature-dependent miscibility measurements with dynamic SIMS show that $PC_{61}BM$ has a more favorable interaction with P3HT relative to PDPP2FT (Fig. 3). Diffusion couples of P3HT/PDPP2FT:deuterated-$PC_{61}BM$ ($dPC_{61}BM$) and PDPP2FT/P3HT:$dPC_{61}BM$ were fabricated and annealed at various temperatures to probe the movement of $dPC_{61}BM$ between the two polymers near melting (T_{melt}) and glass transitions (T_g). In both cases, the neat polymer film was placed on top of the complementary binary blend, and thus the binary blend was initially at a greater depth in the film than the neat polymer layer. Using the detection of deuterium anions, the chemical depth profile of $dPC_{61}BM$ was measured for each annealed sample. Figure 3(a) shows the initial diffusion couple structure before thermal annealing. The sample held at room temperature contains $dPC_{61}BM$ only within the initially mixed PDPP2FT:$dPC_{61}BM$ binary blend and not within the neat P3HT layer, as expected; the same lack of mixing is present in Figure 3(b) at room temperature, where all $dPC_{61}BM$ remains within the initially blended layer with P3HT. However, as the annealing temperature of the bilayer is increased, the two diffusion couples show significantly different behavior. As the temperature is increased above 100 °C for fixed time (5 min), $dPC_{61}BM$ begins to diffuse from the PDPP2FT binary blend to the initially neat P3HT layer, and the volume fraction of fullerene diffusing into P3HT begins to surpass the volume fraction remaining within the PDPP2FT layer at temperatures

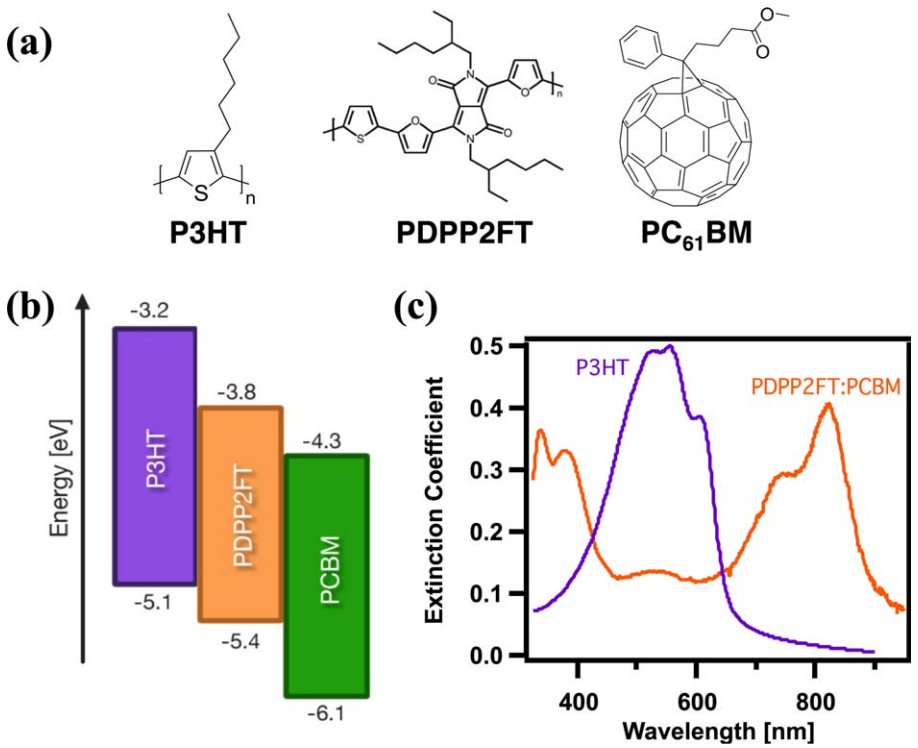

FIGURE 2 (a) Chemical structures of P3HT, PDPP2FT and $PC_{61}BM$. (b) Energy level diagram of cascading ternary blend components.[14,24] (c) UV-Vis absorption spectra of P3HT and PDPP2FT:PCBM thin films.

exceeding 150 °C. On the other hand, it is apparent that the volume fraction of $dPC_{61}BM$ that migrates from P3HT to PDPP2FT remains quite small well into the rubbery and melt states.

The origin of the mixing behavior is not solely due to kinetics. One could assume that the differences in the depth distribution of $PC_{61}BM$ are kinetically controlled because $PC_{61}BM$ is much more mobile in P3HT at the temperatures and time scales probed. While the thermal transition temperatures of the layers vary as a function of composition, we can consider the limits of T_{melt} for the pure materials (~215 °C for P3HT, ~275 °C for $PC_{61}BM$, and ~280 °C for PDPP2FT).[47,48] The bilayer diffusion experiments show mixing of $dPC_{61}BM$ from PDPP2FT to P3HT upon even moderate heating, but little demixing from P3HT into neat PDPP2FT upon aggressive heating. This observation demonstrates the thermodynamic basis of the changes in the depth distribution.

The results show that even at temperatures as high as 230 °C, only a small part of $dPC_{61}BM$ moves from a 1:1 P3HT:$dPC_{61}BM$ blend into the pure PDPP2FT layer, while a pure P3HT layer draws substantial amounts of $dPC_{61}BM$ out of a 1:1 PDPP2FT:$dPC_{61}BM$ blend. Even at temperatures as low as 150 °C, already more $dPC_{61}BM$ can be found in the initially pure P3HT layer than in the initially blended PDPP2FT layer [see Fig. 3(a)]. Due to the substantial amount (50 wt %) of $dPC_{61}BM$ within the source layer, significant diffusion also results in a change of the thickness of both layers, leading to a shift of the interface in the dynamic SIMS measurements, indicated by the full and dashed black lines in the raw data plots (Supporting Information Fig. S3). The same interface shift was also verified by the change in the polymer's characteristic sulfur (^{34}S) signal.

Additionally, the constant $dPC_{61}BM$ concentration throughout the initially neat P3HT layer after annealing indicates that there is no kinetic limitation to the diffusion process on the time scale investigated (5 min). Once the T_g of PDPP2FT is surpassed, the fullerene has sufficient free volume and thus molecular mobility to traverse to the P3HT layer, as is thermodynamically preferred. At temperatures of 150 °C and higher, the composition of $dPC_{61}BM$ in the P3HT layer is relatively constant with depth. Moreover, the volume fraction of $dPC_{61}BM$ within the P3HT layer increases incrementally with annealing temperature because the solubility of the fullerene in amorphous P3HT is temperature-controlled, as we have shown previously.[43] As can be seen in Figure 3(b), while $dPC_{61}BM$ is able to diffuse within the P3HT film at elevated temperatures (above T_g for P3HT), the volume fraction that has traversed into PDPP2FT remains low even close to its melt temperature. This low mixed volume fraction is not due to the lack of molecular mobility of $dPC_{61}BM$ but instead is caused by the very low solubility of the fullerene in PDPP2FT relative to its solubility in P3HT, even at temperatures approaching the melt state. This experiment clearly demonstrates that the differences in fullerene miscibility in

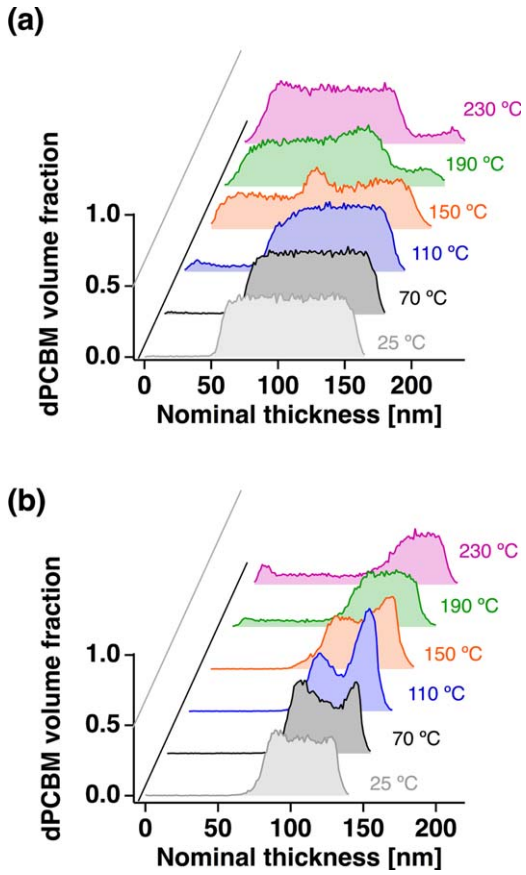

FIGURE 3 Dynamic SIMS depth profiles of bilayers of (a) neat-P3HT/PDPP2FT:dPC$_{61}$BM and (b) neat-PDPP2FT/P3HT:dPC$_{61}$BM (first polymer is closest to the origin) after annealing at the indicated temperature for 5 min.

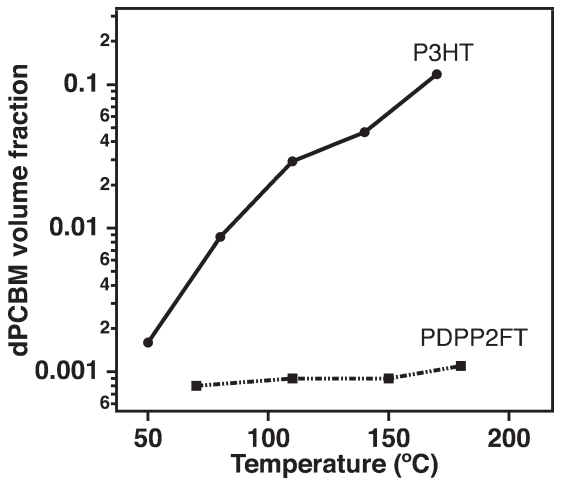

FIGURE 4 Volume fraction of dPC$_{61}$BM in P3HT and PDPP2FT as a function of annealing temperature for bilayer diffusion couples.

semiconducting polymers such as P3HT and PDPP2FT are not a consequence of slow diffusion kinetics, but are in fact based on solubility.[49]

These measurements of interdiffusion also provide insight on the contrasting, empirically derived optimal blend ratios for the two binary mixtures P3HT:PC$_{61}$BM (~1:1) and PDPP2FT:PC$_{61}$BM (~1:3) in studies of solar cells.[14,50] There have been recent suggestions that a "three-phase" morphology with both pure and mixed domains is beneficial for charge generation and transport in BHJs.[51–53] At first consideration, it might appear from these blend ratios that PC$_{61}$BM is very soluble in PDPP2FT, and the higher level of PC$_{61}$BM is required in order to force the fullerene to form aggregated domains for electron transport. Such an argument would suggest that P3HT has lower solubility for PC$_{61}$BM and therefore requires less fullerene content to develop aggregated domains. However, as our measurements clearly indicate, the solubility of PC$_{61}$BM is significantly higher in P3HT than in PDPP2FT (Fig. 4). This preferential blending suggests that, instead, a high level of PC$_{61}$BM may be required to drive it into the amorphous regions of PDPP2FT. It is assumed here that PC$_{61}$BM resides only within amorphous regions of P3HT (not within crystallites),[43] and that PDPP2FT is more disordered (as observed by GIWAXS).

Our results from dynamic SIMS indicate that, in the solid state, there is a strong preference for PC$_{61}$BM to segregate into P3HT relative to PDPP2FT. We note that formation of BHJs during solution casting is a kinetically limited process and that there are other factors, such as aggregation in solution, that are at play.[54–57] Our results do suggest that in a ternary BHJ, there is a possibility that regions of PDPP2FT will be depleted of PC$_{61}$BM, which will reduce the interfacial area that is critical for charge generation. This is particularly likely with post processing steps such as thermal annealing. We therefore fabricated ternary BHJs over a range of compositions to study their optoelectronic properties and morphology to understand how our results from model diffusion couples could be used to understand the properties of solution cast BHJs.

Optoelectronic Properties of Ternary Bulk Heterojunctions

Before considering a ternary blend, it is important to consider the endpoints of the binary BHJs, P3HT:PC$_{61}$BM and PDPP2FT:PC$_{61}$BM. Both binary blends have comparable PCE in photovoltaic solar cells when processed under literature conditions. We obtained average PCEs of 3.0% and 3.1% in 1:0.7 P3HT:PC$_{61}$BM and 1:3 PDPP2FT:PC$_{61}$BM cells, respectively, close to reported values for these materials.[14,50] Overall, while the fill factor (FF) for P3HT:PC$_{61}$BM is considerably higher than that of PDPP2FT:PC$_{61}$BM, the performance is offset by the slightly higher open-circuit voltage (V_{OC}) and J_{SC} of the latter (see Supporting Information). It should be noted that, the processing conditions required to achieve 3.0% and 3.1% in binary BHJs do not necessarily translate to ternary BHJs, and we have chosen a set of processing conditions and compositions for ternary cells that we believe emphasize morphological changes over absolute performance.

The operation of a ternary BHJ with an energy cascade structure [Fig. 2(b)] is significantly more complex than that of a binary BHJ.[42] In a ternary blend BHJ, carrier generation can occur at interfaces of the polymers with $PC_{61}BM$ and also between polymers (see Supporting Information Fig. S1). The photogenerated carriers may or may not explore all phases during charge extraction. For example, if there are well-separated domains of the polymers (greater than the film thickness in size), holes residing on PDPP2FT could reach the electrode before finding an energetically more stable state in P3HT (based on the smaller IE of P3HT). A similar issue occurs for electrons between PDPP2FT and $PC_{61}BM$. In this case, the domains may behave more like BHJs that are electrically parallel (although clearly they share molecular interfaces and cannot be strictly electrically "parallel"). If the domains are mixed, or small, then the carriers can access states in all the materials before extraction. This case has been discussed as "delocalized"[32,42] and leads to optoelectronic performance similar to an alloy. The optoelectronic characteristics of the BHJ therefore can provide clues as to the morphology.

To examine the optoelectronic performance of ternary BHJ solar cells with P3HT and PDPP2FT, we examined the properties of devices with varying blend ratios, such that the weight ratio of fullerene to total polymer was similar to that in an optimal binary mixture (Fig. 5). To form these BHJs solutions of P3HT:PCBM in a 1:0.7 ratio and PDPP2FT: $PC_{61}BM$ in a 1:3 ratio were mixed to achieve various weight ratios of polymer. This procedure kept the ratio of $PC_{61}BM$ to each polymer at that of each "optimal" binary endpoint. The ternary BHJs were annealed at 110 °C before testing where our dynamic SIMS data begins to show significant diffusion (Fig. 3).

The performance of the ternary blends can be compared to the binary endpoints. As the weight ratio of PDPP2FT is increased from a binary blend of P3HT:$PC_{61}BM$, the FF and J_{SC} of the solar cells both decrease significantly until ~50 wt % PDPP2FT. In this same range of compositions, the V_{OC} increases, especially above ~30 wt % PDPP2FT. Focusing now on the right side of Figure 5, where PDPP2FT comprises the entire donor polymer fraction, mixing P3HT into PDPP2FT:$PC_{61}BM$ first improves then deteriorates performance as the weight fraction of P3HT is increased. The V_{OC} increases nearly linearly with P3HT content until greater than 50 wt % polymer, while the FF increases until ~80 wt % PDPP2FT then deteriorates. The J_{SC} increases slightly and is approximately constant up to ~10 wt % P3HT but then strongly decreases. Thus it is clear that blending P3HT into the PDPP2FT:$PC_{61}BM$ at low ratios results in optimal performance of these ternary devices; however, over-addition of P3HT (>25 wt %) disrupts the photocurrent generated and leads to significant deterioration of performance. Similar enhancements in performance near the endpoints of composition have been observed in other ternary blends.[58]

The behavior of some ternary BHJs has been based on an alloy model where the V_{oc} is linearly (or nearly so) dependent on composition and results from occupancy of hole states of the blended donors.[42] Here, we see a linear dependence in one region of composition (above 50 wt % PDPP2FT) and a nearly independent region below that with a relatively sharp transition in between. This behavior can be understood as follows. At low concentrations of PDPP2FT, the V_{oc} is essentially that of P3HT:$PC_{61}BM$, and therefore transport is dominantly in P3HT and $PC_{61}BM$. There is a substantial increase in V_{oc} near 50 wt % PDPP2FT to a V_{oc} of 0.8 V, which is higher than either of the endpoints. While this may seem striking, it is likely an indication that P3HT is disordered in the ternary blend at this composition and higher. If we consider alloying behavior previously observed in other ternary blends,[42] the V_{oc} would extrapolate to 0.92 V at 0 wt % PDPP2FT based on the linear regime. This is nearly equivalent to the reported V_{oc} of regio-random P3HT:$PC_{61}BM$ of ~0.9 V.[59,60] These results therefore suggest that upon blending of the PDPP2FT:$PC_{61}BM$ solution at sufficient levels, the ordering of P3HT is hindered in the resulting ternary BHJ. This loss of ordering results in an increased IE, and thus increased V_{OC}, relative to the fixed $PC_{61}BM$ LUMO.[59] In this region of composition, it is also suggestive that the domain sizes are small enough for holes to explore

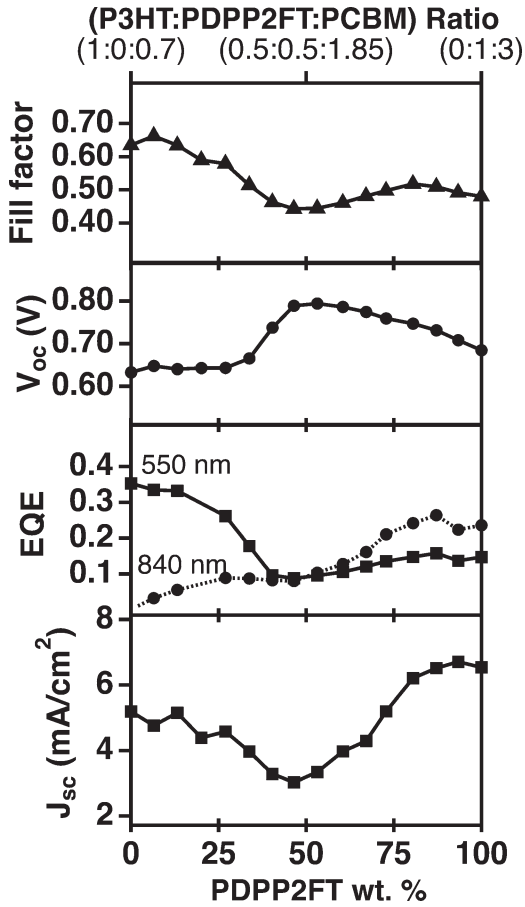

FIGURE 5 Values of FF, V_{OC}, J_{SC}, and wavelength-specific EQE of the compositionally varying ternary blend system. Devices were annealed at 110 °C and the parameters are averages of five devices.

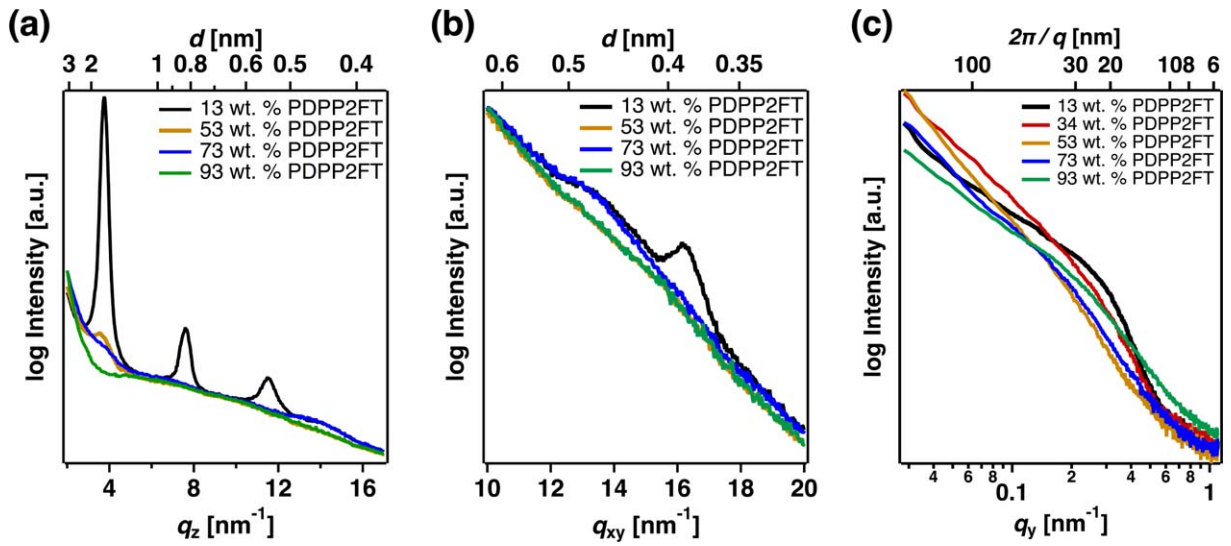

FIGURE 6 GIWAXS, out-of-plane (a) and in-plane (b) integrations, showing the loss of P3HT crystallinity as PDPP2FT content is increased in thermally annealed thin films. GISAXS in-plane (c) integrations of the same blends, highlighting the change in domain separation length scale as the blend composition is varied. Thin films were annealed at 110 °C for 5 min.

electronic states formed by both polymers. In the compositional region where there is no dependence on addition of PDPP2FT (below 50 wt %), the independence suggests that holes do not explore both polymers. This implies that there are little to no carriers in PDPP2FT, preventing the observation of an alloying effect. In this analysis we are assuming that electrons are only transported in $PC_{61}BM$ due to the large offset (~0.5 eV) with the EA of PDPP2FT.

We can further use external quantum efficiency (EQE) data to support the picture of the morphology suggested by the changes in V_{oc} with composition. Also presented in Figure 5 are the composition-dependent EQE values at 550 nm and 840 nm excitation, wavelengths corresponding to absorption features specific to ordered P3HT and PDPP2FT, respectively. As PDPP2FT is blended to higher levels, approaching an equal weight proportion of each polymer, the EQE in the PDPP2FT absorption band increases slightly as expected, but the P3HT-specific EQE drops dramatically. This reduction in photocurrent generated by P3HT again originates from the disordering of P3HT as PDPP2FT is added.

The intermixing and optoelectronic characteristics of the ternary BHJs provide a view of the morphology of the films. A likely origin of the disordering of P3HT is the mismatch in the miscibility of $PC_{61}BM$ in the two polymers. P3HT is more likely to be rich in $PC_{61}BM$ than PDPP2FT, and this difference could prevent crystallization during casting from solution. We therefore examined the morphology directly using grazing incidence X-ray scattering (GIXS) to gain more information about the structure of the ternary BHJs.

Morphology of Ternary Blends

In order to understand the changes in characteristics of the ternary BHJs as a function of composition, we performed GIXS characterization. Grazing incidence wide angle X-ray scattering (GIWAXS) provided information on the ordering of both polymer phases and grazing incidence small angle X-ray scattering (GISAXS) on the length scales of phase separation. We find evidence that corroborates the inferences about the morphology from the measurements of devices.

GIWAXS reveals that the structural order of P3HT in the ternary blends varies as a function of composition. Vertical (thin film out-of-plane) and horizontal (in-plane) integrations of GIWAXS patterns are given in Figure 6. The (200) and (300) scattering peaks of P3HT are only present at low PDPP2FT loadings, and only a weak (100) shoulder is visible at higher composition. The (010) π-stacking peak near 17 nm^{-1} of P3HT is only observed at low composition of PDPP2FT as well. These data agree well with the inferences about the structural order of P3HT from the solar cell measurements that suggested disordering of P3HT at high weight ratios of PDPP2FT. Clearly the intensity of the scattering should vary with composition, but it should be possible to observe ordered domains of P3HT at the 53 wt % ratio if there was similar crystallinity to the binary blend.

In addition to changes in local ordering, the ternary blend composition affects the length scale of domain separation from GISAXS [Fig. 6(c)]. The ternary BHJ nominally contains five regions that pervade the ternary BHJ morphology, which are relatively pure domains of each material, P3HT, PDPP2FT, and $PC_{61}BM$, and mixed domains of polymer and fullerene (P3HT + $PC_{61}BM$ and PDDP2FT + $PC_{61}BM$), and potentially intermixed polymer. As the composition is varied, scattering observed in SAXS changes from primarily that of polymer- and fullerene-rich domains near the binary composition limits to primarily that of P3HT and PDDP2FT domains at intermediate compositions.

We consider the compositional limits in turn. Horizontal line integrations of GISAXS data provide evidence of a thin film domain structure that originates from both polymer-fullerene domain separation and polymer-polymer domain separation [Figs. 1 and 6(c)]. Near the binary composition limits, differences in density between polymer- and fullerene-loaded amorphous domains form average correlations of 10 to 50 nm, typical of well-performing BHJs. At intermediate compositions (25–50 wt % PDPP2FT) scattering at low-$\boldsymbol{q}$ values is enhanced, presumably from a longer length scale phase separation (>100 nm) typical of polymers. In addition, near 50 wt % PDPP2FT, $PC_{61}BM$ preferentially swells P3HT regions relative to those of PDPP2FT, resulting in large, swollen domains containing P3HT and a large local concentration of $PC_{61}BM$. At 73 wt % PDPP2FT, the lower concentration of P3HT prevents it from containing high levels of $PC_{61}BM$ and suppresses the formation of P3HT- and $PC_{61}BM$-rich domains; thus, the microstructure at that composition is dominated by PDPP2FT- and $PC_{61}BM$-rich domain formation. Therefore, compared to 53 wt % PDPP2FT, this 73 wt % blend shows decreased scattering at low-$\boldsymbol{q}$ values, corresponding to a loss of the larger (100–150 nm) domain structure. At this composition, scattering from domain correlations is weakest, because the more strongly scattering P3HT-$PC_{61}BM$ and P3HT-PDPP2FT domain structures (relative to PDPP2FT-$PC_{61}BM$ domains) are suppressed. In addition, it is at this blend ratio that the ternary mixture is most compositionally uniform, with the mismatch in miscibilities leading to relatively proportionate local blending within amorphous regions of each polymer. This morphology is consistent with the alloying behavior observed for the V_{oc}.

Understanding the Compositional Dependence of Ternary BHJs

Based on our optoelectronic and morphological data on the P3HT:PDPP2FT:$PC_{61}BM$ ternary BHJs, we can revisit the schematic morphology of Figure 1. One expects that PDPP2FT and P3HT will phase separate during solvent removal during spin-casting of the BHJ. Due to their different compatibility with $PC_{61}BM$, the P3HT domains likely accumulate a much larger amount of $PC_{61}BM$ than the PDPP2FT domains. Ordering in P3HT is suppressed by larger volume fractions of $PC_{61}BM$ as the PDPP2FT binary is added to the P3HT binary, based on the concentrations used to form the ternary BHJs in this work. Upon thermal annealing, our model dynamic SIMS experiments on diffusion couples suggest that $PC_{61}BM$ will likely further accumulate in regions rich in P3HT even at low temperatures and short times (e.g. 5 min) of annealing. This effect will be particularly pronounced if the P3HT regions are disordered before annealing, due to $PC_{61}BM$ intermixing primarily in amorphous P3HT regions.[43,53] Thus, one must consider both the miscibility of the fullerene with multiple donor polymers and the resulting blend structure in designing and predicting the performance of ternary BHJs.

To understand the compositional behavior in the ternary system, we first consider perturbation of the binary P3HT:$PC_{61}BM$. Upon addition of small amounts of PDPP2FT, the added donor domains will contain little $PC_{61}BM$ due to the much higher miscibility of $PC_{61}BM$ in P3HT than in PDPP2FT. At PDPP2FT ratios below 25 wt %, the added fraction of PDPP2FT leads to a decrease in J_{sc}, suggesting there is poor charge generation due to inefficient mixing with $PC_{61}BM$. At PDPP2FT ratios of 25 to 50 wt %, the excess $PC_{61}BM$ leads to the destruction of P3HT crystallinity (Fig. 6) and an increase in V_{OC} due to the expected deepening of the IE at the same time. There is no benefit to the PCE due to the drop in FF and J_{sc}, caused by inefficient charge generation by PDPP2FT and the blue-shift in the absorbance of P3HT. At higher PDPP2FT ratios of 50 to 75 wt %, the effect is inverted, and performance begins to recover. The decreasing amount of amorphous P3HT likely allows some $PC_{61}BM$ to migrate back into PDPP2FT domains, and the length scale of domain separation is smaller, allowing the performance to improve (higher FF and J_{sc}).

The best performance of the ternary is achieved in a small compositional range. In a very narrow window above 75 wt % PDPP2FT, addition of P3HT leads to a beneficial effect. Because there is not enough P3HT present to deplete a significant amount of $PC_{61}BM$ from the PDPP2FT regions, the PDPP2FT:$PC_{61}BM$ part of the active layer is fully operational. The amorphous P3HT leads to a slight increase in V_{OC} without affecting the other parameters, and as a consequence leads to a small increase in the PCE. Deviations from alloying behavior in the V_{oc} have been observed previously near the endpoints of composition, which are close to binary systems.[20,42,58] Here we see a smooth trend which is likely due to the domain sizes observed in GISAXS, but such data has not been reported for many ternary systems, making it hard to compare the results directly.

It is useful to consider another ternary system that can test the potential generality of the mismatch of fullerene miscibility in controlling the thin film microstructure and device performance. For comparison, the ternary system, P3HT:Si-PCPDTBT:$PC_{61}BM$, with an energy cascade structure has been previously studied by Ameri et al.[18] and found to yield well-performing solar cells. In particular, by adding Si-PCPDTBT to the binary bulk heterojunction P3HT:$PC_{61}BM$, the V_{OC}, J_{SC}, and PCE were found to increase consistently over a broad range of compositions (up to 70 wt % Si-PCPDTBT). In this case, we find that the performance enhancement conforms to our hypothesis that more closely matched polymer-fullerene miscibilities are required in order to produce a clear enhancement in the PCE of ternary blends. Figure S5 in the Supporting Information displays the comparison of $PC_{61}BM$ miscibility, determined by dynamic SIMS in P3HT, PDPP2FT, and Si-PCPDTBT. The relative miscibilities of P3HT and Si-PCPDTBT are far closer than those of P3HT and PDPP2FT, suggesting that there is less of a mismatch in the fullerene composition of amorphous polymer-rich domains in the ternary bulk heterojunction involving

P3HT and Si-PCPDTBT. The V_{oc} changes smoothly with composition for this system, in contrast to the results here, suggesting that the P3HT stays ordered throughout.[18] This comparison of the change in device characteristics and the miscibility of the fullerene in the donor polymers further supports our conclusion that the compatibility of each polymer with $PC_{61}BM$ is a critical parameter in the performance of ternary BHJ OPVs. Previous work has discussed the importance of the compatibility between donor polymers to observe smooth changes in V_{oc} with composition.[33] Our work here shows that the behavior can be more complex if one of the polymers has a significant change in IE with structural order, like P3HT.

CONCLUSIONS

In conclusion, analysis of the electrical characteristics and morphology of the ternary system PDPP2FT:P3HT:$PC_{61}BM$ enables an understanding of the effect of composition and morphology on the behavior of ternary BHJs to be developed. Our results highlight the role of the miscibility of the fullerene acceptor with each donor polymer and reveal the impact on optoelectronic properties. The complex behavior of the open circuit voltage with composition shows that simple mixing rules can be strongly affected by morphology. As a result, it is important to consider both the miscibility of the donors and fullerene and the impact on ordering of polymers when evaluating new candidates for ternary blend cells. For pairs of polymers with similar miscibility with $PC_{61}BM$, there is a better chance to maintain the nanostructure required for charge generation in ternary BHJs.

ACKNOWLEDGMENTS

The authors thank the SAXS/WAXS team at Beamline 7.3.3 of the Advanced Light Source at Lawrence Berkeley National Lab for their help with the GIWAXS and GISAXS measurements, including Eric Schaible, Ilja Gunkel, and Chenhui Zhu. This report is based upon work supported by the National Science Foundation under Grant no. 1207549. This work made use of UCSB Materials Research Laboratory Central Facilities, supported by the MRSEC Program of the National Science Foundation under award no. DMR 1121053. The Advanced Light Source is supported by the Director, Office of Science, Office of Basic Energy Sciences, of the U.S. Department of Energy under Contract no. DE-AC02-05CH11231. M.A. Brady acknowledges support from National Science Foundation and California NanoSystems Institute Graduate Research Fellowships and an Advanced Light Source Doctoral Fellowship. N.D. Treat acknowledges support from the NSF's International Research Fellowship Program (OISE-1201915) and the European Research Council's Marie Curie International Incoming Fellowship under grant agreement No. 300091. This manuscript is dedicated to the memory of Edward J. Kramer, of the University of California, Santa Barbara, for his generous and unwavering support and mentorship of his students, who hope to carry his passion for polymer science and research into the future and inspire the next generation of scientists.

REFERENCES AND NOTES

1 S. Reineke, M. Thomschke, B. Lüssem, K. Leo, *Rev. Mod. Phys.* **2013**, *85*, 1245–1293.

2 A. C. Arias, J. D. MacKenzie, I. McCulloch, J. Rivnay, A. Salleo, *Chem. Rev.* **2010**, *110*, 3–24.

3 A. Facchetti, *Mater. Today* **2013**, *16*, 123–132.

4 Q., Y. Zhang, W. Sun, D.X. Zhu, *Adv. Mater.* **2014**, *26*, 6829–6851.

5 L. Dou, J. You, Z. Hong, Z. Xu, G. Li, R. A. Street, Y. Yang, *Adv. Mater.* **2013**, *25*, 6642–6671.

6 J. Roncali, P. Leriche, P. Blanchard, *Adv. Mater.* **2014**, *26*, 3821–3838.

7 F. C. Krebs, N. Espinosa, M. Hösel, R. R. Søndergaard, M. Jørgensen, *Adv. Mater.* **2014**, *26*, 29–39.

8 M. A. Green, K. Emery, Y. Hishikawa, W. Warta, E. D. Dunlop, *Prog. Photovolt. Res. Appl.* **2013**, *21*, 1–11.

9 Y. Liu, J. Zhao, Z. Li, C. Mu, W. Ma, H. Hu, K. Jiang, H. Lin, H. Ade, H. Yan, *Nat. Commun.* **2014**, *5*, 1–8.

10 R. A. J. Janssen, J. Nelson, *Adv. Mater.* **2013**, *25*, 1847–1858.

11 N. E. Jackson, B. M. Savoie, T. J. Marks, L. X. Chen, M. A. Ratner, *J. Phys. Chem. Lett.* **2015**, *6*, 77–84.

12 N. D. Treat, M. L. Chabinyc, *Ann. Rev. Phys. Chem.* **2014**, *65*, 59–81.

13 H. Lu, B. Akgun, T. P. Russell, *Adv. Energy Mater.* **2011**, *1*, 870–878.

14 C. H. Woo, P. M. Beaujuge, T. W. Holcombe, O. P. Lee, J. M. J. Fréchet, *J. Am. Chem. Soc.* **2010**, *132*, 15547–15549.

15 A. T. Yiu, P. M. Beaujuge, O. P. Lee, C. H. Woo, M. F. Toney, J. M. J. Fréchet, *J. Am. Chem. Soc.* **2012**, *134*, 2180–2185.

16 M. C. Scharber, M. Koppe, J. Gao, F. Cordella, M. A. Loi, P. Denk, M. Morana, H. J. Egelhaaf, K. Forberich, G. Dennler, R. Gaudiana, D. Waller, Z. Zhu, X. Shi, C. J. Brabec, *Adv. Mater.* **2010**, *22*, 367–370.

17 M. J. Robb, S. Y. Ku, F. G. Brunetti, C. J. Hawker, *J. Polym. Sci. Part A: Polym. Chem.* **2013**, *51*, 1263–1271.

18 T. Ameri, J. Min, N. Li, F. Machui, D. Baran, M. Forster, K. J. Schottler, D. Dolfen, U. Scherf, C. J. Brabec, *Adv. Energy Mater.* **2012**, *2*, 1198–1202.

19 M. C. Chen, D. J. Liaw, Y. C. Huang, H. Y. Wu, Y. Tai, *Sol. Energy Mater. Sol. Cells* **2011**, *95*, 2621–2627.

20 P. P. Khlyabich, B. Burkhart, B. C. Thompson, *J. Am. Chem. Soc.* **2012**, *134*, 9074–9077.

21 Y. Kim, S. Cook, S. A. Choulis, J. Nelson, J. R. Durrant, D. D. C. Bradley, *Synth. Met.* **2005**, *152*, 105–108.

22 H. Kim, M. Shin, Y. Kim, *J. Phys. Chem. C.* **2009**, *113*, 1620–1623.

23 M. Koppe, H. J. Egelhaaf, G. Dennler, M. C. Scharber, C. J. Brabec, P. Schilinsky, C. N. Hoth, *Adv. Funct. Mater.* **2010**, *20*, 338–346.

24 L. M. Kozycz, D. Gao, J. Hollinger, D. S. Seferos, *Macromolecules* **2012**, *45*, 5823–5832.

25 F. Machui, S. Rathgeber, N. Li, T. Ameri, C. J. Brabec, *J. Mater. Chem.* **2012**, *22*, 15570–15577.

26 S. J. Park, J. M. Cho, W. B. Byun, J. C. Lee, W. S. Shin, I. N. Kang, S. J. Moon, S. K. Lee, *J. Polym. Sci. Part A: Polym. Chem.* **2011**, *49*, 4416–4424.

27 T. Ameri, T. Heumüller, J. Min, N. Li, G. Matt, U. Scherf, C. J. Brabec, *Energy Environ. Sci.* **2013**, *6*, 1796–1801.

28 R. Lin, M. Wright, B. P. Veettil, A. Uddin, *Synth. Met.* **2014**, *192*, 113–118.

29 Y. Yang, W. Chen, L. Dou, W. H. Chang, H. S. Duan, B. Bob, G. Li, Y. Yang, *Nat. Photonics* **2015**, *9*, 190–198.

30 P. P. Khlyabich, A. E. Rudenko, B. Burkhart, B. C. Thompson, *ACS Appl. Mater. Int.* **2015**, *7*, 2322–2330.

31 S. Kouijzer, W. Li, M. W. Wienk, R. A. J. Janssen, *J. Photonics Energy* **2014**, *5*, 057203.

32 R. A. Street, P. P. Khlyabich, A. E. Rudenko, B. C. Thompson, *J. Phys. Chem. C* **2014**, *118*, 26569–26576.

33 P. P. Khlyabich, A. E. Rudenko, R. A. Street, B. C. Thompson, *ACS Appl. Mater. Int.* **2014**, *6*, 9913–9919.

34 M. Koppe, H. J. Egelhaaf, E. Clodic, M. Morana, L. Lüer, A. Troeger, V. Sgobba, D. M. Guldi, T. Ameri, C. J. Brabec, *Adv. Energy Mater.* **2013**, *3*, 949–958.

35 C. Kästner, S. Rathgeber, D. A. M. Egbe, H. Hoppe, *J. Mater. Chem. A* **2013**, *1*, 3961–3969.

36 S. Y. Chang, H. C. Liao, Y. T. Shao, Y. M. Sung, S. H. Hsu, C. C. Ho, W. F. Su, Y. F. Chen, *J. Mater. Chem. A* **2013**, *1*, 2447–2452.

37 P. P. Khlyabich, B. Burkhart, A. E. Rudenko, B. C. Thompson, *Polymer* **2013**, *54*, 5267–5298.

38 L. Yang, L. Yan, W. You, *J. Phys. Chem. Lett.* **2013**, *4*, 1802–1810.

39 Y. Gu, C. Wang, F. Liu, J. Chen, O. E. Dyck, G. Duscher, T. P. Russell, *Energy Environ. Sci.* **2014**, *7*, 3782–3790.

40 P. P. Khlyabich, A. E. Rudenko, B. C. Thompson, Y.-L. Loo, *Adv. Funct. Mater.*, **2015**, DOI: 10.1002/adfm.201502287.

41 L. Lu, M. A. Kelly, W. You, L. Yu, *Nat. Photonics* **2015**, *9*, 491–500.

42 R. A. Street, D. Davies, P. P. Khlyabich, B. Burkhart, B. C. Thompson, *J. Am. Chem. Soc.* **2013**, *135*, 986–989.

43 N. D. Treat, M. A. Brady, G. Smith, M. F. Toney, E. J. Kramer, C. J. Hawker, M. L. Chabinyc, *Adv. Energy Mater.* **2011**, *1*, 82–89.

44 N. D. Treat, A. Varotto, C. J. Takacs, N. Batara, M. Al-Hashimi, M. J. Heeney, A. J. Heeger, F. Wudl, C. J. Hawker, M. L. Chabinyc, *J. Am. Chem. Soc.* **2012**, *134*, 15869–15879.

45 M. J. Robb, D. Montarnal, N. D. Eisenmenger, S. Y. Ku, M. L. Chabinyc, C. J. Hawker, *Macromolecules* **2013**, *46*, 6431–6438.

46 T. Ameri, P. Khoram, J. Min, C. J. Brabec, *Adv. Mater.* **2013**, *25*, 4245–4266.

47 S. Malik, A. K. Nandi, *J. Polym. Sci. Part B: Polym. Phys.* **2002**, *40*, 2073–2085.

48 P. E. Hopkinson, P. A. Staniec, A. J. Pearson, A. D. F. Dunbar, T. Wang, A. J. Ryan, R. A. L. Jones, D. G. Lidzey, A. M. Donald, *Macromolecules* **2011**, *44*, 2908–2917.

49 D. Leman, M. A. Kelly, S. Ness, S. Engmann, A. Herzing, C. Snyder, H. W. Ro, R. J. Kline, D. M. DeLongchamp, L. J. Richter, *Macromolecules* **2015**, *48*, 383–392.

50 W. Ma, C. Yang, X. Gong, K. Lee, A. J. Heeger, *Adv. Funct. Mater.* **2005**, *15*, 1617–1622.

51 F. C. Jamieson, E. B. Domingo, T. McCarthy-Ward, M. Heeney, N. Stingelin, J. R. Durrant, *Chem. Sci.* **2012**, *3*, 485–492.

52 T. M. Burke, M. D. McGehee, *Adv. Mater.* **2014**, *26*, 1923–1928.

53 B. A. Collins, E. Gann, L. Guignard, X. He, C. R. McNeill, H. Ade, *J. Phys. Chem. Lett.* **2010**, *1*, 3160–3166.

54 M. M. Wienk, M. Turbiez, J. Gilot, R. A. J. Janssen, *Adv. Mater.* **2008**, *20*, 2556–2560.

55 V. S. Gevaerts, A. Furlan, M. M. Wienk, M. Turbiez, R. A. J. Janssen, *Adv. Mater.* **2012**, *24*, 2130–2134.

56 W. Li, W. S. C. Roelofs, M. Turbiez, M. M. Wienk, R. A. J. Janssen, *Adv. Mater.* **2014**, *26*, 3304–3309.

57 M. A. Brady, G. M. Su, M. L. Chabinyc, *Soft Matter* **2011**, *7*, 11065–11077.

58 L. Lu, T. Xu, W. Chen, E. S. Landry, L. Yu, *Nat. Photonics* **2014**, *8*, 716–722.

59 K. Vandewal, A. Gadisa, W. D. Oosterbaan, S. Bertho, F. Banishoeib, I. V. Severen, L. Lutsen, T. J. Cleij, D. Vanderzande, J. V. Manca, *Adv. Funct. Mater.* **2008**, *18*, 2064–2070.

60 S. Ko, E. T. Hoke, L. Pandey, S. Hong, R. Mondal, C. Risko, Y. Yi, R. Noriega, M. D. McGehee, J. L. Brédas, A. Salleo, Z. Bao, *J. Am. Chem. Soc.* **2012**, *134*, 5222–5232.